Report RU-TR-MAE-203-F

Large Eddy Simulation of Three-Dimensional High Speed Aerodynamic Flows

Final Technical Report
1 August 1996 – 30 November 1998

AFOSR Grant F49620-96-1-0389

Prof. Doyle D. Knight
Department of Mechanical and Aerospace Engineering
Rutgers University - The State University of New Jersey
98 Brett Road · Piscataway, NJ 08854-8058
Phone: 732 445 4464 · Fax: 732 445 5313
Email: knight@jove.rutgers.edu

Submitted to:
Dr. Len Sakell
Air Force Office of Scientific Research
801 N. Randolph St., Rm 732
Arlington, Virginia 22203-1977

March 1, 1999

SECURITY CLASSIFICATION OF THIS PAGE

AFRL-SR-BL-TR-99-

0101

REPORT DOCUMENTATION

1a. REPORT SECURITY CLASSIFICATION Unclassified	1b. RESTRICTIVE
2a. SECURITY CLASSIFICATION AUTHORITY	3. DISTRIBUTION / AVAILABILITY OF REPORT Approved for public release Distribution unlimited
2b. DECLASSIFICATION / DOWNGRADING SCHEDULE	
4. PERFORMING ORGANIZATION REPORT NUMBER(S) RU-TR-MAE-F-203	5. MONITORING ORGANIZATION REPORT NUMBER(S)
6a. NAME OF PERFORMING ORGANIZATION Dept of Mech and Aeo Engr Rutgers University 6b. OFFICE SYMBOL (If applicable)	7a. NAME OF MONITORING ORGANIZATION Air Force Office of Scientific Research
6c. ADDRESS (City, State, and ZIP Code) 98 Brett Road Piscataway, NJ 08854-8058	7b. ADDRESS (City, State, and ZIP Code) 801 N. Randolph St., Rm. 732 Arlington, VA 22203-1977
8a. NAME OF FUNDING / SPONSORING ORGANIZATION AF Office of Scien. Research 8b. OFFICE SYMBOL (If applicable)	9. PROCUREMENT INSTRUMENT IDENTIFICATION NUMBER F49620-96-1-0389
8c. ADDRESS (City, State, and ZIP Code) 801 N. Randolph St., Rm 732 Arlington, VA 22203-1977	10. SOURCE OF FUNDING NUMBERS PROGRAM ELEMENT NO. 2307AS; PROJECT NO.; TASK NO.; WORK UNIT ACCESSION NO.

11. TITLE (Include Security Classification)
Large Eddy Simulation of High Speed Aerodynamic Three Dimensional Flows

12. PERSONAL AUTHOR(S)
Doyle Knight

13a. TYPE OF REPORT	13b. TIME COVERED	14. DATE OF REPORT (Year, Month, Day)	15. PAGE COUNT
Final	FROM 96/08/01 TO 98/11/30	99/03/01	23

16. SUPPLEMENTARY NOTATION

17. COSATI CODES			18. SUBJECT TERMS (Continue on reverse if necessary and identify by block number)
FIELD	GROUP	SUB-GROUP	High speed flows; computational fluid dynamics; turbulence large eddy simulatios; unstructured grid; parallel computing

19. ABSTRACT (Continue on reverse if necessary and identify by block number)

An unstructured grid Large Eddy Simulation (LES) methodology has been developed for compressible high speed flows. The filtered compressible Navier-Stokes equations are solved on an unstructured grid of tetrahedra. The inviscid fluxes are obtained from an exact locally one-dimensional Riemann solver using Godunov's method. The viscous fluxes are obtained using a discrete analog of Gauss' Theorem. The reconstruction is performed using a Least Squares technique. The temporal integration is a Runge-Kutta method. The algorithm is overall second order accurate in space and time. Four flowfields have been computed: decay of isotropic turbulence, channel flow, supersonic flat plate boundary layer and supersonic compression corner. The first and second cases are effectively incompressible, while the third and fourth cases are supersonic (Mach 3). The computed results show close agreement with experiment and Direct Numerical Simulation, and validate the unstructured grid LES methodology.

20. DISTRIBUTION / AVAILABILITY OF ABSTRACT ☒ UNCLASSIFIED/UNLIMITED ☐ SAME AS RPT. ☐ DTIC USERS	21. ABSTRACT SECURITY CLASSIFICATION Unclassified
22a. NAME OF RESPONSIBLE INDIVIDUAL	22b. TELEPHONE (Include Area Code) / 22c. OFFICE SYMBOL

DD FORM 1473, 84 MAR 83 APR edition may be used until exhausted. All other editions are obsolete.

SECURITY CLASSIFICATION OF THIS PAGE
Unclassified

Abstract

An unstructured grid Large Eddy Simulation (LES) methodology has been developed for compressible high speed flows. The filtered compressible Navier-Stokes equations are solved on an unstructured grid of tetrahedra. The inviscid fluxes are obtained from an exact locally one-dimensional Riemann solver using Godunov's method. The viscous fluxes are obtained using a discrete analog of Gauss' Theorem. The reconstruction is performed using a Least Squares technique. The temporal integration is a Runge-Kutta method. The algorithm is overall second order accurate in space and time. Four flowfields have been computed: decay of isotropic turbulence, channel flow, supersonic flat plate boundary layer and supersonic compression corner. The first and second cases are effectively incompressible, while the third and fourth cases are supersonic (Mach 3). The computed results show close agreement with experiment and Direct Numerical Simulation, and validate the unstructured grid LES methodology.

Table of Contents

Introduction

The effective design of high speed aircraft and missiles depends critically upon accurate prediction of aerodynamic and aerothermodynamic performance which are strongly affected by flow turbulence under most flight conditions. From an engineering standpoint, the aircraft or missile aerodynamicist needs the capability for accurate prediction of the mean and rms fluctuating surface pressure ($\bar{p}_w$ and p'_w) and surface heat transfer ($\bar{q}_w$ and q'_w), mean surface skin friction ($\bar{\tau}_w$), and locations of primary and secondary separation.

Table 1 RANS Capability for 3-D Shock Wave Boundary Layer Interaction

Quantity	*Satisfactory*	*Unsatisfactory*	*No capability shown*
$\bar{p}_w$	√		
p'_w			√
$\bar{q}_w$		√	
q'_w			√
Primary Separation	√		
Secondary Separation		√	

The current methodology for prediction of compressible turbulent flows is based on the Reynolds-averaged Navier-Stokes (RANS) equations (Knight 1993). This approach has yielded a hierarchy of turbulence models extending from zero-equation to full Reynolds Stress Equation models. While these models have generally been capable of predicting the engineering quantities of interest in weakly perturbed boundary layers, they have been unable to accurately predict the complex 3-D flows which are encountered in highly maneuvering, high angle-of-attack flight. Two recent extensive reviews have documented the capabilities and deficiencies of a wide range of RANS models for prediction of complex 3-D flows with shock wave-turbulent boundary layer interactions (Knight 1997, Knight and Degrez 1998). The results, summarized in Table 1, indicate that a significant number of critical engineering quantities are not capable of prediction by current RANS models. Therefore, more advanced turbulence models are needed which have the ability to simulate the complex physics of turbulence with greater generality.

Large Eddy Simulation (LES) is an alternative to RANS hich may be capable of predicting more (or all) of the aerodynamic and aerothermodynamic quantities of engineering interest described above. In LES, the governing equations are spatially filtered on the scale of the numerical grid. The large, energy-containing eddies are directly computed. These eddies are strongly influenced by the physical geometry and configuration of the flow. Thus, the direct computation of the large eddies by LES, as opposed to the modeling of the large eddies by RANS, gives greater generality, in principle, to LES. The influence of the unresolved scales of motion is simulated using a subgrid-scale (SGS) model (Smagorinsky 1963, Lilly 1967, Deardorff 1970, Germano *et al* 1991, Piomelli *et al* 1991, Ghosal *et al* 1995) or by the inherent dissipation in the numerical scheme (Boris *et al* 1992, Oran and Boris 1993, Porter *et al* 1994, Grinstein 1996, Ansari and Strang 1996). Because the statistics of the small scale turbulence are expected to be more homogeneous and isotropic than those of the large scales, a general model of the small scales seems more plausible than a general model of the entire spectrum of turbulent motions.

LES has been shown to be both a useful research tool for understanding the physics of turbulence, and also a predictive method for flows of engineering interest. Recent compendia and reviews include Galperin and Orszag (1993), Mason (1994), Lesieur and Métais (1996) and Moin (1997). Many models have been developed for the subgrid-scale stress tensor. These include the conventional Smagorinsky eddy viscosity model (Smagorinsky 1963, Lilly 1967, Deardorff 1970), the spectra eddy viscosity model of Kraichnan (1976), the dynamic SGS model of Germano *et al* (1991), the scale similarity model of Bardina *et al* (1980), and the localized dynamic SGS model of Ghosal *et al* (1995) and more recently of Menon and Kim (1996), and many others. Although most research has focused on incompressible turbulent flows, there has recently emerged a growing interest in applications of LES to compressible turbulent flows. Examples include Yoshizawa (1986), Speziale *et al* (1988), Moin *et al* (1991), Erlebacher *et al* (1992), Zang *et al* (1992), El-Hady *et al* (1994), Jansen (1997), Spyropoulos and Blaisdell (1996), and Haworth and Jansen (1996). Nearly all compressible LES has employed spectral methods or structured grids, with the exception of Jansen and Haworth.

Apart from the complexities of the flowfield, the complicated geometries of high speed vehicles is also a challenge. To enable treatment of complex geometries and also achieve high resolution of the flowfield dynamically, we employ an unstructured grid. There are two important advantages of unstructured grids. First, algorithms have been developed to facilitate automatic generation of unstructured grids for a complex geometries (see, for example, the discussion in Barth (1990, 1992). These grid generation methods can be substantially more efficient (in terms of user time) than some of the multi-block structured grid generation methods used. Second, local mesh refinement, either adaptive or fixed, can been performed much more readily for unstructured grids.

The report summarizes the research in Large Eddy Simulation of compressible turbulent flows using unstructured grids. Two methods for simulation of the subgrid scale stresses have been examined. The first method is the Monotone Integrated Large Eddy Simulation (MILES) technique. The second method is a hybrid technique combining MILES with a Smagorinsky eddy viscosity model for the subgrid scale stresses. These two methods, together with different algorithms for the inviscid fluxes and function reconstruction, have been evaluated for four turbulent flows: the decay of isotropic incompressible turbulence, channel flow, supersonic boundary layer and supersonic compression corner. The results are in overall good agreement with the experiment and Direct Numerical Simulation (DNS), thereby validating the accuracy of the methodology.

Governing Equations

The governing equations are the three-dimensional filtered Navier-Stokes equations. For a function f, its filtered form $\bar{f}$ is

$$\bar{f} \equiv \frac{1}{V}\int_V G f dV$$

where G is the filtering function, and its Favre-averaged form $\tilde{f}$ is

$$\tilde{f} \equiv \frac{\overline{\rho f}}{\bar{\rho}}$$

where ρ is the density. From the Navier-Stokes equations for the instantaneous flow variables density (ρ), velocity in the ith coordinate direction (u_i), pressure (p) and temperature (T), Favre-averaging and spatial filtering yield the filtered Navier-Stokes equations (here written using the Einstein summation notation where repeated indices denote summation)

$$\frac{\partial \bar{\rho}}{\partial t} + \frac{\partial \bar{\rho}\tilde{u}_k}{\partial x_k} = 0$$

$$\frac{\partial \bar{\rho}\tilde{u}_i}{\partial t} + \frac{\partial \bar{\rho}\tilde{u}_i\tilde{u}_k}{\partial x_k} = -\frac{\partial \bar{p}}{\partial x_i} + \frac{\partial \mathcal{T}_{ik}}{\partial x_k}$$

$$\frac{\partial \bar{\rho}\tilde{e}}{\partial t} + \frac{\partial}{\partial x_k}(\bar{\rho}\tilde{e} + \bar{p})\tilde{u}_k = \frac{\partial \mathcal{Q}_k}{\partial x_k} + \frac{\partial}{\partial x_k}(\mathcal{T}_{ik}\tilde{u}_i)$$

$$\bar{p} = \bar{\rho}R\tilde{T}$$

where

$$\mathcal{T}_{ik} = \tau_{ik} + \bar{\sigma}_{ik}$$

$$\tau_{ik} = -\bar{\rho}(\widetilde{u_i u_k} - \tilde{u}_i\tilde{u}_k)$$

$$\bar{\sigma}_{ik} = \mu(\tilde{T})\left(-\tfrac{2}{3}\frac{\partial \tilde{u}_j}{\partial \tilde{x}_j}\delta_{ik} + \frac{\partial \tilde{u}_i}{\partial x_k} + \frac{\partial \tilde{u}_k}{\partial x_i}\right)$$

$$\mathcal{Q}_k = Q_k + \bar{q}_k$$

$$Q_k = -\bar{\rho}c_p(\widetilde{Tu_k} - \tilde{T}\tilde{u}_k)$$

$$\bar{q}_k = k(\tilde{T})\frac{\partial \tilde{T}}{\partial x_k}$$

$$\bar{\rho}\tilde{e} = \bar{\rho}c_v\tilde{T} + \tfrac{1}{2}\bar{\rho}\tilde{u}_i\tilde{u}_i + \bar{\rho}\tilde{k}$$

$$\bar{\rho}\tilde{k} = \tfrac{1}{2}(\overline{\rho u_i u_i} - \bar{\rho}\tilde{u}_i\tilde{u}_i) = -\tfrac{1}{2}\tau_{ii}$$

Two different Sub-Grid-Scale (SGS) models are employed. The first model is Monotone Integrated Large Eddy Simulation (MILES) wherein the numerical algorithm itself provides the requisite dissipation associated with the subgrid scale motions. The second model is the classical constant-coefficient Smagorinsky method

$$\tilde{S}_{ij} = \tfrac{1}{2}\left(\frac{\partial \tilde{u}_i}{\partial \tilde{x}_j} + \frac{\partial \tilde{u}_j}{\partial \tilde{x}_i}\right)$$
$$\tau_{ij} = 2C_R\bar{\rho}\Delta^2\sqrt{\tilde{S}_{mn}\tilde{S}_{mn}}\left(\tilde{S}_{ij} - \tfrac{1}{3}\tilde{S}_{kk}\delta_{ij}\right)$$
$$Q_j = \bar{\rho}c_p\frac{C_R}{Pr_t}\Delta^2\sqrt{\tilde{S}_{mn}\tilde{S}_{mn}}\,\frac{\partial \tilde{T}}{\partial x_j}$$

where $C_R = 0.00423$ and Δ is the length scale which is related to the local grid size. For boundary layer flows, Δ is multiplied by the Van Driest damping factor

$$D = 1 - e^{-n^+/A}$$

where $A = 26$, $n^+ = nu_\tau/\nu_w$ is the normal distance to the (nearest) solid boundary normalized by the viscous length scale ν_w/u_τ where ν_w is the kinematic viscosity evaluated at the wall and U_τ is the local friction velocity.

We simplify the notation by hereafter dropping the tilde $\tilde{}$ and overbar $\bar{}$. The flow variables are nondimensionalized using the reference density ρ_∞, velocity U_∞, static temperature T_∞ and length scale L, with Mach number $M_\infty = U_\infty/\sqrt{\gamma RT_\infty}$. The governing equations are therefore

$$\frac{\partial \rho}{\partial t} + \frac{\partial \rho u_k}{\partial x_k} = 0$$
$$\frac{\partial \rho u_i}{\partial t} + \frac{\partial \rho u_i u_k}{\partial x_k} = -\frac{\partial p}{\partial x_i} + \frac{\partial \mathcal{T}_{ik}}{\partial x_k}$$
$$\frac{\partial \rho e}{\partial t} + \frac{\partial}{\partial x_k}(\rho e + p)u_k = \frac{\partial}{\partial x_k}(\mathcal{Q}_k + \mathcal{T}_{ik}u_i)$$
$$p = \frac{\rho T}{\gamma M_\infty^2}$$

Numerical Algorithm

The governing equations are expressed in finite volume form for a control volume V with surface ∂V

$$\frac{d}{dt}\int_V Q dV + \int_{\partial V}(F\hat{\imath} + G\hat{\jmath} + H\hat{k})\cdot\hat{n}dA = 0$$

where Q is the vector of dependent variables

$$Q = \begin{Bmatrix} \rho \\ \rho u \\ \rho v \\ \rho w \\ \rho e \end{Bmatrix}$$

and the flux vectors are

$$F = \begin{Bmatrix} \rho u \\ \rho u^2 + p - \mathcal{T}_{xx} \\ \rho uv - \mathcal{T}_{xy} \\ \rho uw - \mathcal{T}_{xz} \\ (\rho e + p)u - \mathcal{Q}_x - \beta_x \end{Bmatrix}, \quad G = \begin{Bmatrix} \rho v \\ \rho uv - \mathcal{T}_{xy} \\ \rho v^2 + p - \mathcal{T}_{yy} \\ \rho vw - \mathcal{T}_{yz} \\ (\rho e + p)v - \mathcal{Q}_y - \beta_y \end{Bmatrix}, \quad H = \begin{Bmatrix} \rho w \\ \rho uw - \mathcal{T}_{xz} \\ \rho vw - \mathcal{T}_{yz} \\ \rho w^2 + p - \mathcal{T}_{zz} \\ (\rho e + p)w - \mathcal{Q}_z - \beta_z \end{Bmatrix}$$

with

$$\beta_x = \mathcal{T}_{xx}u + \mathcal{T}_{xy}v + \mathcal{T}_{xz}w$$
$$\beta_y = \mathcal{T}_{xy}u + \mathcal{T}_{yy}v + \mathcal{T}_{yz}w$$
$$\beta_z = \mathcal{T}_{xz}u + \mathcal{T}_{yz}v + \mathcal{T}_{zz}w$$

An unstructured grid of tetrahedra is employed, with a cell-centered storage architecture. The cell-averaged values, stored at the centroid of each tetrahedron of volume V_i are

$$Q_i = \frac{1}{V_i}\int_{V_i} Q dV$$

The inviscid fluxes are computed using Godunov's method which is an exact one-dimensional Riemann solver (Gottlieb and Groth 1988) applied normal to each face. The inviscid flux computations require the values of each variable on either side of the cell faces. These values are obtained from the cell-averaged values by second-order or third-order function reconstruction using the Least Squares method of Ollivier-Gooch (Ollivier-Gooch 1997). The second-order function reconstruction method of Frink (1994) was employed in some of the earlier LES studies, but was found inferior to the method of Ollivier-Gooch (Okong'o and Knight 1998). More details on the reconstruction schemes are given in Okong'o and Knight (1998).

The viscous fluxes and heat transfer are computed by application of Gauss' theorem to the control volume whose vertices are the centroids of the cells which share each node. The second-order accurate scheme (in 2-D) is given by Knight (1994) and the extension to 3-D is straightforward.

Parallelization

The code is parallelized using domain decomposition and Message Passing Interface (MPI). Domain decomposition is performed in a pre-processing step. The domain is decomposed in a single direction with equal number of tetrahedra in each domain. A halo of cells is added in each domain to provide data on the adjacent domain, and the halo cell data is updated at every subiterate of the time integration. An example is shown in Fig. 1 for the LES of decay of isotropic turbulence. The numerical algorithm achieves excellent parallel performance. For example, the speed-up on four processors of the SGI Power Onyx with R-10000 processors is 3.7 for 93% efficiency (Knight *et al* 1998).

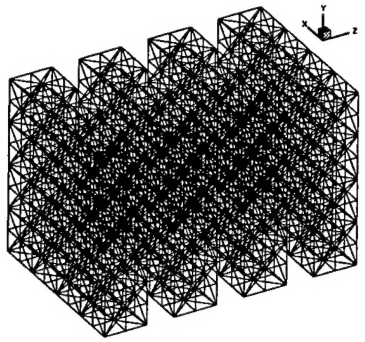

Fig. 1 Example of domain decomposition

Results

Four different configurations have been examined: decay of isotropic turbulence, channel flow, flat plate boundary layer and supersonic compression corner. The first and second cases are effectively incompressible, while the third and fourth cases are supersonic (Mach 3).

Decay of Isotropic Turbulence

The benchmark experiment by Comte-Bellot and Corrsin (CBC) (1971) of the decay of isotropic turbulence was selected to examine the following specific issues of the unstructured grid LES code: the MILES *vs* hybrid SGS models, the method for reconstruction of the flow variables to the cell faces, the demonstration of achieving consistent results using two different grids, the type of Riemann solver, regular *vs* random grids, the convergence parameter in Godunov's method, and the number of Fourier intervals used in the initial spectrum. In the experiment, turbulence was generated using a biplane, square rod grid with mesh size $M = 5.08$ cm and solidity of 0.34 in a uniform mean flow of velocity $U_0 = 10$ m/s. The Reynolds number based on the grid spacing is $Re = 34000$. The measurements were performed downstream of the grid at three locations, $U_0 t/M = 42$, 98, and 171 where t is the dimensional "time" in the experiment. The computation was performed in a periodic box. Details are presented in Knight *et al* (1998).

Ten different computations, as summarized in Table 2, were performed to evaluate the issues described below. Cases 1 through 7 and 10 use the MILES model (*i.e.*, no SGS model), while Cases 8 and 9 use the hybrid model (*i.e.*, MILES plus the Smagorinsky SGS model). Case 1 employs a) second-order least-squares reconstruction with 8 cells in the stencil, b) a regular grid, c) Godunov's method, d) a convergence parameter of 10^{-10} in Godunov's method, and e) $N_k = 26$ in the initial energy spectrum. Cases 2 through 7 in succession modify one of these five choices. For example, Case 2 employs Frink's method for reconstruction. Cases 8 and 9 use the hybrid (MILES plus Smagorinsky models) with different length scale Δ. The Smagorinsky constant C_R is chosen to be 0.012. Cases 1 to 9 employ Grid 1, and Case 10 employs Grid 2.

Table 2 Decay of Isotropic Turbulence

Case	*Grid*	*SGS Model*	Δ	*Reconstruction Method*	*Grid Type*	N_k	*Riemann Solver*	*Toler*
1	1	MILES	n/a	LS 2nd	Reg	26	Godunov	10^{-10}
2	1	MILES	n/a	F 2nd	Reg	26	Godunov	10^{-10}
3	1	MILES	n/a	F 2nd	Reg	26	Roe	
4	1	MILES	n/a	First	Reg	26	Godunov	10^{-10}
5	1	MILES	n/a	F 2nd	Ran	26	Godunov	10^{-10}
6	1	MILES	n/a	F 2nd	Reg	26	Godunov	10^{-12}
7	1	MILES	n/a	F 2nd	Reg	52	Godunov	10^{-10}
8	1	Hybrid		F 2nd	Reg	26	Godunov	10^{-10}
9	1	Hybrid		F 2nd	Reg	26	Godunov	10^{-10}
10	2	MILES	n/a	F 2nd	Reg	26	Godunov	10^{-10}

Legend

Grid 1	No. of tetrahedra = 163,840
Grid 2	No. of tetrahedra = 1,310,720
MILES	Monotone Integrated Large Eddy Simulation (Boris *et al* 1992)
LS 2nd	Second order least-squares reconstruction method
F 2nd	Second order Frink's reconstruction method
First	First order reconstruction method
Reg	Regular grid of tetrahedra
Ran	Grid obtained by random perturbing the nodes of the regular grid
N_k	Number of Fourier intervals used for initial energy spectrum
Toler	Tolerance employed in iteration solution for p^*

The decay of the resolved turbulence kinetic energy for Cases 1 to 9 is compared with the filtered experimental data of CBC in Fig. 2. The MILES method using either second order reconstruction method (Cases 1 to 3, and 5 to 7) accurately predicts the turbulence decay. This remarkable result implies that the inherent numerical dissipation in the numerical algorithm (due to the finite order accuracy of the reconstruction and quadrature) provides a reasonable model of turbulent energy dissipation. The computations employing the hybrid (MILES plus Smagorinsky models) exhibit only a small difference compared to the MILES simulations, since the dissipation of turbulence energy is almost entirely a consequence of the numerical algorithm (MILES).

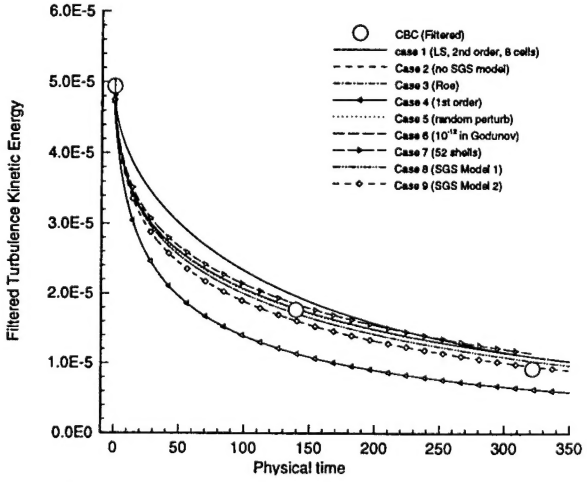

Fig. 2 Filtered turbulent kinetic energy

The computation using the second order least-squares method (Case 1) shows a lower decay rate than those using Frink's method (Cases 2, 3, and 5 to 7). The second order least-squares evidenlty has a lower inherent numerical dissipation than the second order Frink's reconstruction. An SGS model may be needed to compensate the reduced inherent numerical dissipation in order to achieve the best agreement with experiment. The computation using the first order reconstruction (Case 4) shows poor agreement with experiment as anticipated.

The MILES approach yields consistent results when the grid is refined (Knight *et al* 1998). The results using either Roe's method (Case 3) or Godunov's method (Case 2) are essentially identical. This is expected since the velocity fluctuations are small compared to the speed of sound.

The choice of regular *vs* random grids has no significant effect on the accuracy of the computation as seen in Fig. 2. where the turbulence energy for Cases 2 and 5 are essentially identical. Moreover, the variation in the convergence parameter used in Godunov's method (Cases 2 and 6), and the number of Fourier intervals in the initial condition (Cases 2 and 7) have negligible effect.

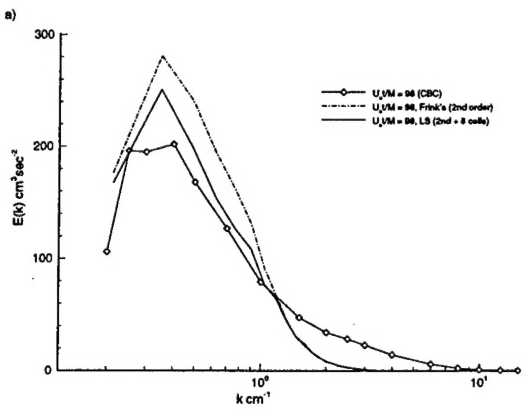

Fig. 3 Energy spectrum at $U_0t/M = 98$

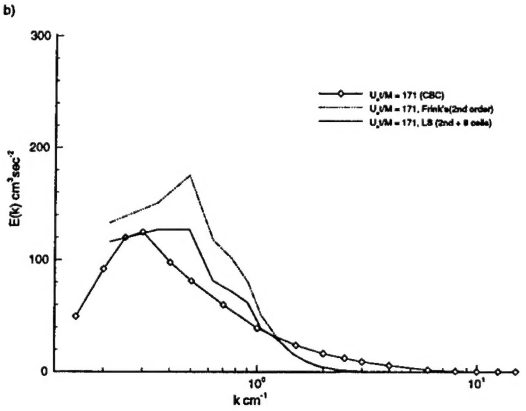

Fig. 4 Energy spectrum at $U_0t/M = 171$

The effect of the functional reconstruction method on the turbulence energy spectrum is shown in Figs. 3 and 4 where the experimental data and computed results using the second order least-squares and Frink's method are shown at $U_0t/M = 98$ and 171, respectively, for Grid 1. The least-squares reconstruction is observed to be more accurate than Frink's method. Since the CPU time for the two methods is approximately the same, the least-squares reconstruction is preferable. A "pile-up" of energy at lower wave numbers is noted. This was also observed by Haworth and Jansen (1996) who employed a similar grid resolution.

Channel Flow

The Reynolds number based on the channel height and bulk velocity is 5600. The Mach number is 0.5; however, the static temperature variation across the channel is small (less than 4%) so the flow is effectively incompressible. The mean flow is in the $x-$ direction, with y and z representing wall normal and spanwise directions, respectively.

Computations have been performed using the constant-coefficient Smagorinsky sub-grid scale model (C_R = 0.012, Pr_t= 0.4). The coefficient C_R is multiplied by the van Driest damping factor $1 - e^{-y^+/26}$ to integrate to the walls. The length scale Δ for the SGS model is the nodal spacing in the y-direction. A body-force is applied in this direction and is adjusted at each timestep to keep the bulk velocity constant. Using the global x-momentum conservation for fully developed flow, $f_1 = -2u_\tau^2$. The bulk velocity is also the reference velocity and so is set equal to 1. The boundary conditions are periodic in the streamwise (x) and spanwise (z) directions with no-slip boundaries in the wall-normal (y) direction, with isothermal walls.

The grid size is $2\pi \times 1 \times 2\pi/3$, where the lengths have been non-dimensionalized by the channel height. The grid has $65 \times 65 \times 65$ nodes (274,625 nodes), 1,310,720 cells, and 2,646,016 faces. The grid is stretched in the y-direction, with minimum spacing (at the walls) of 0.00278 and a maximum spacing (in the channel center) of 0.0457. The initial condition is obtained from interpolating the fully-developed solution on a grid with

$33 \times 65 \times 33$ nodes with the same wall-normal (y) spacing but double the streamwise and spanwise spacing. The flow has been simulated for about twenty-two flow-through times, with statistics accumulated over the last twelve flow-through times. (One flow-through time is the domain length in the x-direction divided by the bulk velocity, i.e., 2π.) The results are compared with the experimental results of Eckelmann (1974) and Kreplin and Eckelmann (1974) and Direct Numerical Simulation of Kim *et al* (1987). In the presentation of results, statistics are accumulated at all grid points. Planar averages are obtained by averaging at all points on planes parallel to the walls, thus making the statistics functions of the wall-normal (y) direction only.

The computed friction velocity, normalized by the bulk velocity, is $u_\tau = 0.0594$ which is within 8% of the DNS and experimental values of 0.0643. The planar average of the time-averaged streamwise velocity U is shown in Figs. 5 and 6. The centerline velocity is 1.155 which is within 0.6% of the experimental value of 1.162. The LES is close to the DNS in the near-wall region, but overshoots it slightly in the core of the channel, consistent with the lower shear stress of the LES. Notably, the LES has excellent agreement with the experimental data of Eckelmann (1979), whose log-law of $u^+ = 2.65 \ln y^+ + 5.9$ is based on data at Re_c of 5600 and 8200. The LES Re_c of about 6470 is between these values. The experimental data points shown in Fig. 6 are for $Re_c = 5600$.

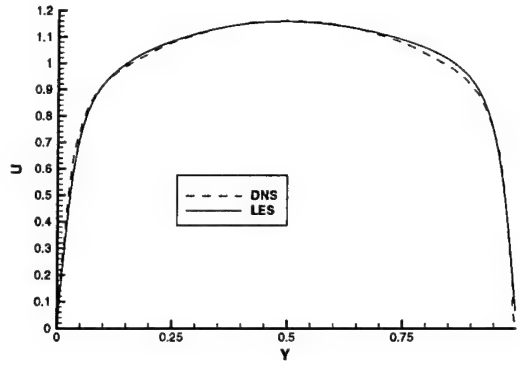

Fig. 5 Mean velocity in entire channel

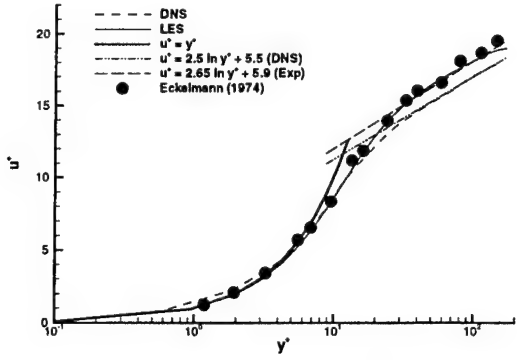

Fig. 6 Mean velocity in wall units

Figs. 7, 8 and 9 compare the root-mean-square velocity fluctuations from the LES with the DNS results of Kim *et al* and the experimental results from Kreplin and Eckelmann (1979). In the experiment, $Re_c = 7700$ and $Re_\tau = 388$, which are slightly higher that the DNS $Re_c = 6600$ and $Re_\tau = 360$ and the LES $Re_c = 6470$ and $Re_\tau = 330$. The velocity fluctuations from the LES, DNS and experiment show generally good agreement. The streamwise fluctuations (Fig. 7) of the LES compare favorably with the experiment, but are slightly higher than the DNS. The LES wall-normal fluctuations to be lower than those of the experiment and DNS (Fig. 8); however, the DNS is also significantly lower than the experiment. The spanwise fluctuations (Fig. 9) show comparable agreement with experiment for the LES and DNS. The computed Reynolds stress, shown in Fig. 10, compares very well with the DNS.

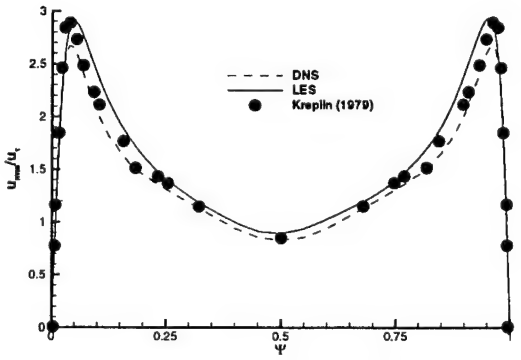

Fig. 7 Rms streamwise velocity fluctuations

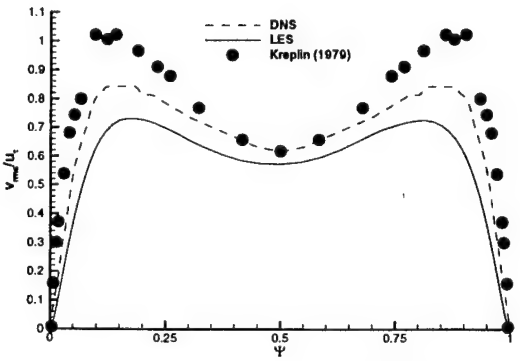

Fig. 8 Rms normal velocity fluctuations

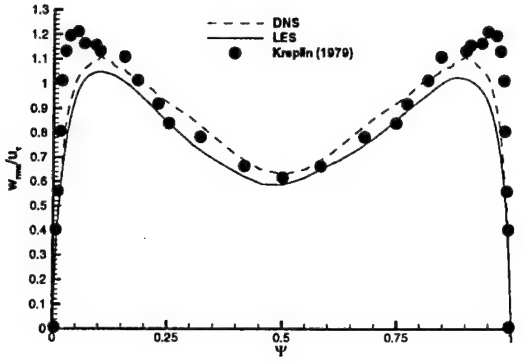

Fig. 9 Rms spanwise velocity fluctuations

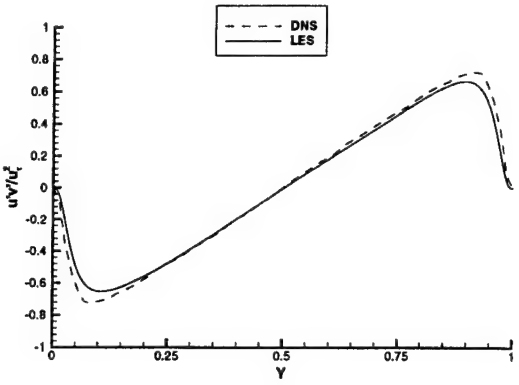

Fig. 10 Reynolds stress

The higher-order velocity statistics based on the resolved velocities are shown in Figs. 11 to 16. The skewness for the streamwise velocity is defined by $S(u') = \overline{u'u'u'}/\overline{u'u'}^{3/2}$ and likewise for v' and w', where the bar denotes the time-average and the prime denotes fluctuation relative to the time-average. Fig. 11 shows the streamwise skewness from the LES to be larger than the DNS, particularly in the center of the channel. The reasons for the disagreement with DNS are under evaluation. However, the agreement for the wall-normal and spanwise skewness, Figs. 12 and 13, is excellent. The flatness for the streamwise velocity is defined by $F(u') = \overline{u'u'u'u}/\overline{u'u'}^2$ and likewise for v' and w'. The streamwise statistics of the LES deviate from the DNS (Fig. 14), while the normal and spanwise flatness profiles, shown in Figs. 15 and 16, agree very well with the DNS.

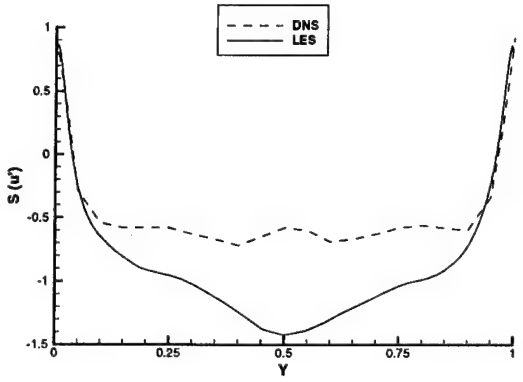

Fig. 11 Streamwise velocity fluctuation skewness

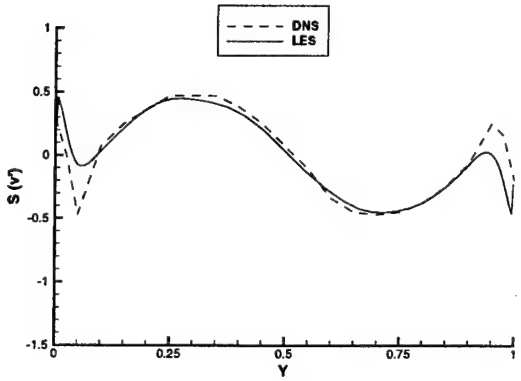

Fig. 12 Normal velocity fluctuation skewness

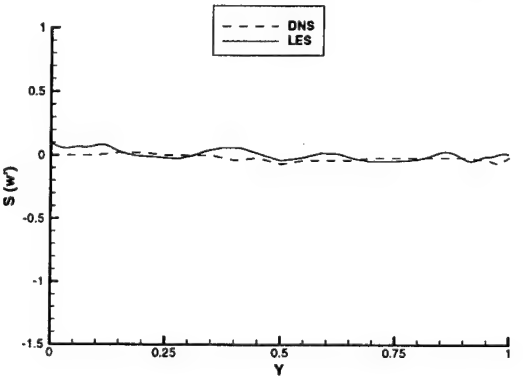

Fig. 13 Spanwise velocity fluctuation skewness

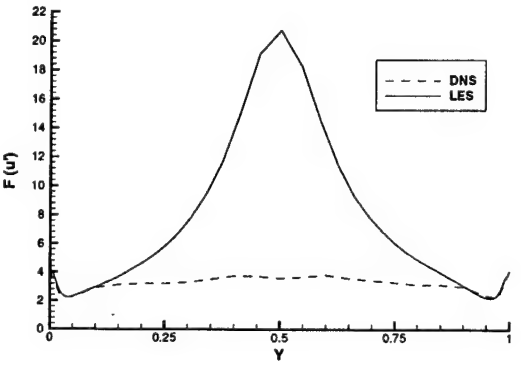

Fig. 14 Streamwise velocity fluctuation flatness

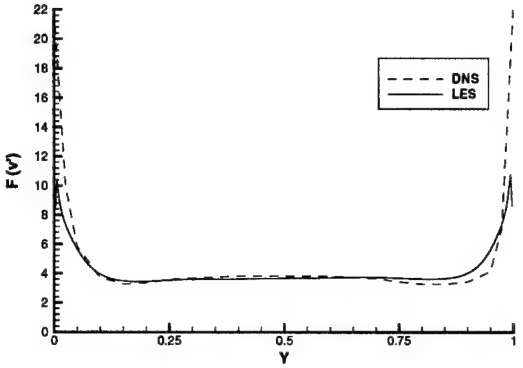

Fig. 15 Normal velocity fluctuation flatness

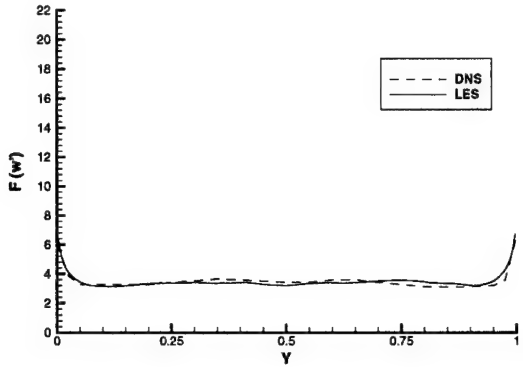

Fig. 16 Spanwise velocity fluctuation flatness

The channel flow LES simulation is effectively MILES, implying that the SGS dissipation is attributable to the numerical algorithm. This is evident in Fig. 17 which shows the Smagorinsky eddy viscosity normalized by the molecular viscosity. The peak value of the Smagorinsky is less than 10% of the molecular viscosity and occurs in the middle of the channel. Thus, the Smagorinsky eddy viscosity does not significantly contribute to the energy dissipation which is due almost entirely to the numerical algorithm. This is a particularly important result and the first observation of this type for an unstructured grid computation of turbulent channel flow.

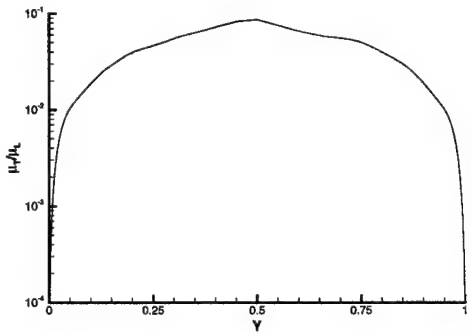

Fig. 17 Smagorinsky eddy viscosity

It is recognized that the above comparison between the DNS and the LES is not precise because the DNS has not been filtered onto the LES grid. However, for this case most of the energy is in the resolved scales, as shown by Fig. 17.

Supersonic Flat Plate Turbulent Boundary Layer

An adiabatic flat plate turbulent boundary layer at Mach 3 and Reynolds number $Re_\delta = 2 \times 10^4$ (based on the incoming boundary layer thickness δ) has been computed. The Reynolds number based on the momentum thickness δ_2 and wall viscosity μ_w is $Re_{\delta_2} = 600$. The Reynolds number is sufficently high to achieve turbulent flow.

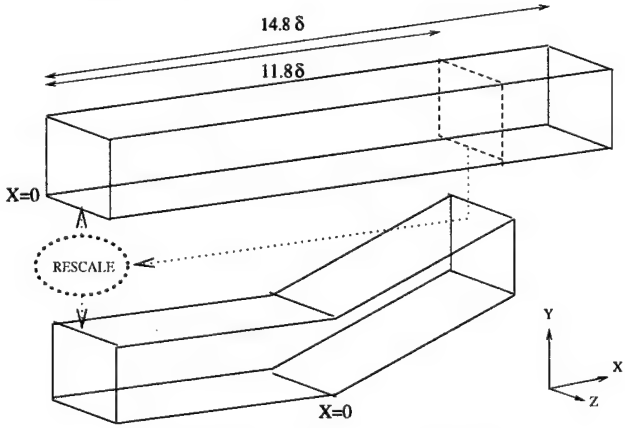

Fig. 18 Computational domain

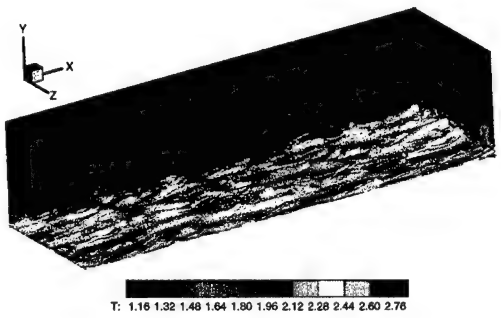

Fig. 19 Instaneous plot of T

The inflow conditions are obtained using a compressible extension of the method of Lund *et al* (1998). The

simulation generates its own inflow conditions through a sequence of operations where the velocity field at a downstream station is rescaled and reintroduced at the inflow boundary (Fig. 18). Defining x, y and z to denote the streamwise, transverse and spanwise directions, respectively, the size of the computational domain is $L_x = 14.8\delta$, $L_y = 3.4\delta$ and $L_z = 4.4\delta$. The spanwise width L_z is approximately six times the experimental spanwise streak spacing (assuming the compressible turbulent boundary layer streaks scale in accordance with incompressible experimental results). The streamwise length L_x is approximately three times the mean experimental streamwise streak size. The height L_y is based on the requirement that acoustic disturbances originating at the upper boundary do not interact with the boundary layer on the lower wall. The grid resolution is 1,600,000 tetrahedral cells. The grid at the wall uses 101×65 nodes. The nodal grid is stretched uniformly in the y using a geometric factor of 1.088. The height Δn of the first cell adjacent to the boundary is less than one wall unit ($\Delta n u_\tau / \nu_w < 1$ where ν_w is the kinematic viscosity at the wall, $u_\tau = \sqrt{\tau_w / \rho_w}$ is the friction velocity, τ_w is the wall shear stress and ρ_w is the density at the wall). The initial condition is a turbulent mean profile with random fluctuations. The simulation is run first for 90 inertial timescales δ / U_∞ in order to eliminate starting transients (Lund *et al* 1998).

Fig. 19 shows the instantaneous temperature contours within the boundary layer. Large turbulent streak-like structures eject high temperature fluid outward the inner layer.

For a function f, its average in time form $< f >$ is defined by

$$< f >= \frac{1}{t_f - t_i} \int_{t_i}^{t_f} f \, dt$$

and its time fluctuating part is

$$f'' = f - < f >$$

In order to provide converged data, the primitive variables are averaged in spanwise direction and the statistical evaluations are perfomed on a period longer than $t_f - t_i = 40\delta / U_\infty$. The notation for the combined temporal and spanwise average is

$$\ll f \gg = \frac{1}{L_z} \frac{1}{t_f - t_i} \int_0^{L_z} \int_{t_i}^{t_f} f \, dt \, dz$$

A simplifying notation is used for the velocity, temperature and pressure

$$U = \ll u \gg$$

The predicted friction velocity is $u_\tau / U_\infty = 0.053$ (the friction coefficient is $c_f = 2.10 \times 10^{-3}$) which is within 3% of the theoretical value of 0.0544 based on the friction law obtained from the combined Law of the Wall and Wake (using the classical coefficients $\kappa = 0.41$; $C = 5.0$; $\Pi = 0.55$). The uncertainty in the experimental data of skin friction is typically $\pm 5\%$, and the accuracy of the correlation is typically $\pm 10\%$ as discussed by Hopkins and Inouye (1971).

The computed adiabatic wall temperature is $T_{aw} / T_\infty = 2.68$ which is within 3% of the theoretical value of $T_{aw} / T_\infty = 2.602$ obtained from the empirical formula

$$\frac{T_{aw}}{T_\infty} = 1 + \frac{(\gamma - 1)}{2} Pr_{t_m} M_\infty^2$$

where $Pr_{t_m} = 0.89$ is the mean turbulent Prandtl number.

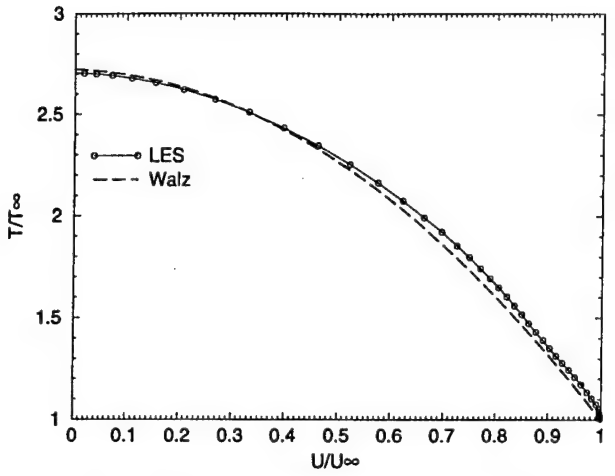

Fig. 20 Mean temperature *vs* velocity

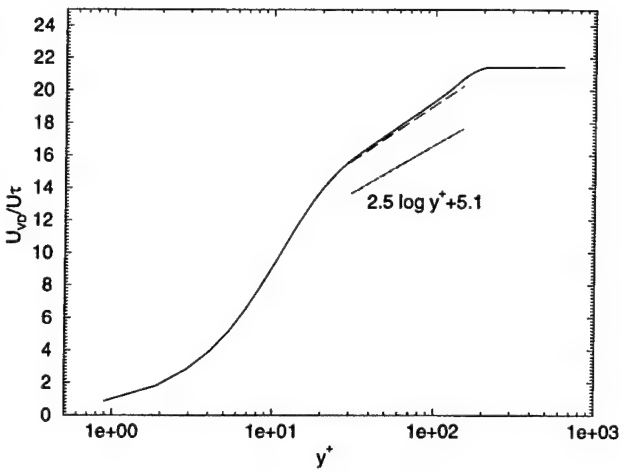

Fig. 21 Mean velocity

In Fig. 20 the temperature-velocity relationship is evaluated. The data fit closely to the classical quadratic profile originally due to Walz (1969).

The log-linear plot of the mean streamwise velocity profile is shown in Fig. 21. The velocity is rescaled according to the Van-Driest transformation and the wall friction velocity. The height y^+ is in wall units. The logarithmic regions appears in the range $30 < y^+ < 150$. In this representation the velocity appears to be over-predicted when compared with the empirical and classical approximation $U_{VD}/U_\tau = 2.5\log(y^+) + 5.1$. The predicted profile fits more accurately with the equation $U_{VD}/U_\tau = 2.9\log(y^+) + 5.7$ (dashed line). In fact, the difference is not as large than it first appears. The representation is very sensitive with the exact friction velocity value (y is measured in wall units, which is wall friction function). If U_τ is assumed to be equal to 0.0598 then the logarithm region will fit perfectly with the classical equation. One explanation of this difference could be the inflow regeneration method that needs to be adjusted accurately (Lund *et al* 1998). Further tests are in progress in order to evaluate the convergence of the constants 2.9 and 5.7 with mesh refinement as well.

Table 3 Flat Plate Boundary Layer Experimental Data

Name	*Mach No.*	Re_δ
LES	3.0	20×10^3
DNS Adams (1997)	3.0	25×10^3
Johnson & Rose (1975)	2.9	1000×10^3
Konrad (1993)	2.9	1590×10^3
Konrad & Smits (1998)	2.87	1900×10^3
Muck *et al* (1984, 1985)	2.87	1638×10^3
Zheltovodov *et al* (1986)	1.7-9.4	up to 2000×10^3

All cases are adiabatic wall

The mean streamwise resolved turbulent kinematic normal stress $\ll u''u'' \gg$, normalized using the local mean density $\ll \rho \gg$ and wall shear stress τ_w, is shown in Fig. 22. As discussed in Zheltovodov and Yakovlev (1986) and Smits and Dussauge (1996), the scaling $\ll \rho \gg \ll u''u'' \gg /\tau_w$ provides an approximate self-similar correlation of experimental data for supersonic flat plate zero pressure gradient adiabatic boundary layers, although the measurements close to the wall are subject to considerable uncertainty. In Fig. 22 data are displayed from Konrad and Smits (1998), Johnson and Rose (1975), Muck *et al* (1984, 1985), Konrad (1993), as well as upper and lower bounds of an extensive set of experimental data for the Mach number range $M = 1.72 - -9.4$ in accordance with generalizations of Zheltovodov and Yakovlev (1986). The characteristics of the different experiments are displayed in Table 3. The computed results show good

agreement with experiment for the main part of the boundary layer ($y/\delta > 0.2$), despite a significantly higher experimental Reynolds number. The decreasing slope corresponds precisely to Johnson and Rose (1975) data. For $y/\delta < 0.2$ the presence of the typical high level peak in the near wall region is supported by experimental data of Konrad (1993) and the Direct Numerical Simulation data from Adams (1997), which is nearly at the same Reynolds number as the LES. However, no conclusion can be drawn about the precise y position and the width of this peak without further experimental data or DNS.

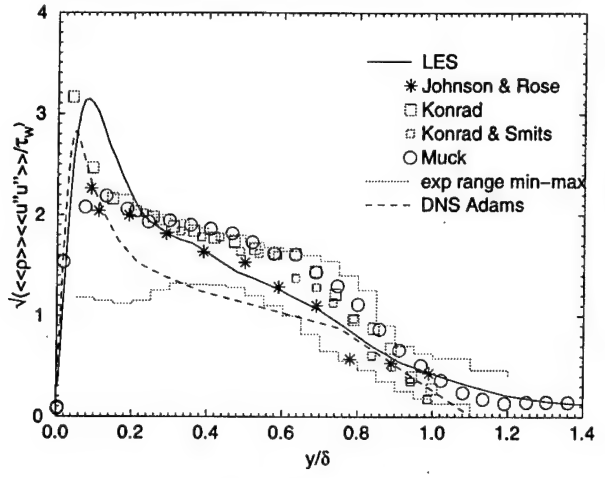

Fig. 22 Reynolds normal stress

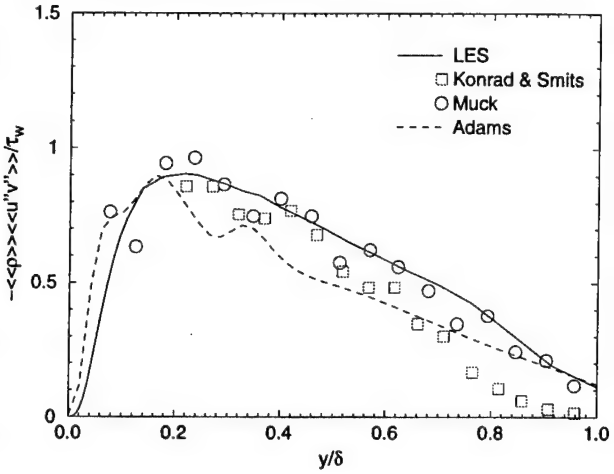

Fig. 23 Reynolds shear stress

In Fig. 23 the Reynolds shear stress distributions are shown for the same experiments and the DNS. Again, the data fit well in the outer part of the boundary layer. The maximum value and the decreasing slope are again well predicted.

Compression Corner

Supersonic flow past a compression corner is an important problem in aerodynamics. It represents, for example, the deflection of a control surface on a wing. The shock can cause a boundary layer separation upstream of the point of impingement of the primary shock, with a secondary shock forming near the separation (Andreopoulos and Muck 1987, Dolling and Or 1983, Horstman *et al* 1977, Settles *et al* 1979, Smits and Muck 1987, Zheltovodov *et al* 1983, Zheltovodov and Yakolev 1986, and Zheltovodov 1996) Reynolds-averaged Navier-Stokes simulations have failed to accurately predict the flow characteristics (Knight and Degrez 1998) such as fluctuating pressure and heat transfer.

Table 4 Compression Corner Experimental Data

Name	α	*Mach*	Re_δ	$Re_{\delta 2}$
LES	8^o	3.0	20×10^3	600
DNS Adams (1997)	18^o	3.0	25×10^3	n/a
Muck *et al* (1984)	8^o	2.87	1638×10^3	40800
Zheltovodov *et al* (1990)	8^o	2.95	75×10^3	2430
Zheltovodov *et al* (1990)	8^o	2.8	110×10^3	3950

All cases are adiabatic wall

David (1993) performed the first LES of a compression corner which successfully reproduced the Taylor-Görtler vortices downstream of the shock. Nevertheless, the use of a pseudo-compressible subgrid-model did not permit accurate quantitative results. The second and most recent LES was Hunt and Nixon (1995) who investigated the role played by turbulence, and showed a direct correlation between the shock motion and the incoming velocity fluctuations. They also demonstrated that the size of the separation bubble has, to some extent, a weak effect on the shock motion. Despite the lack of detail in the inner layer (a log-law wall function was used on a rough grid resolution), it displayed the qualitative features of the shock oscillation

observed experimentally (Dolling and Or 1983).

A computation of an adiabatic turbulent boundary layer flow past a 8° compression corner at Mach 3.0 and $Re_\delta = 2 \times 10^4$ was performed. As indicated in Table 4, the configuration corresponds to the experiments of Zheltovodov and his colleagues except that the Reynolds number is lower for the LES. Table 4 also includes the flow conditions for other experiments and DNS which are reference LES results.

The computational domain is $-6.0\delta \leq x \leq 6.0\delta$ where δ is the incoming boundary layer thickness and x is measured from the corner (Fig. 24). The height and width of the computational domain are $L_y = 3.4\delta$ and $L_z = 4.4\delta$ (*i.e.*, the same lengths as previous flat plate configuration). The grid is 1,600,000 tetrahedral cells. The nodal grid is stretched in the y using a geometric factor of 1.088. The height Δn of the first cell adjacent to the boundary is less than one wall unit.

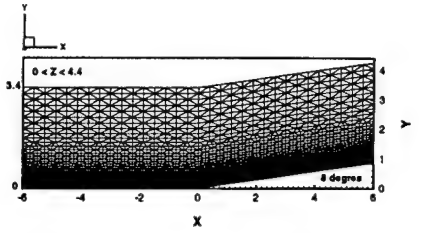

Fig. 24 Computational domain

Inflow data are extracted from the previous flat plate boundary layer LES (Fig. 18). At each time step, the velocity, pressure and temperature fields at the downstream station are rescaled and stored in a datafile. Storage is performed over a period equal to $3L_x/U_\infty$ (equivalent to $36\delta/U_\infty$), which yields about 14 GWords.

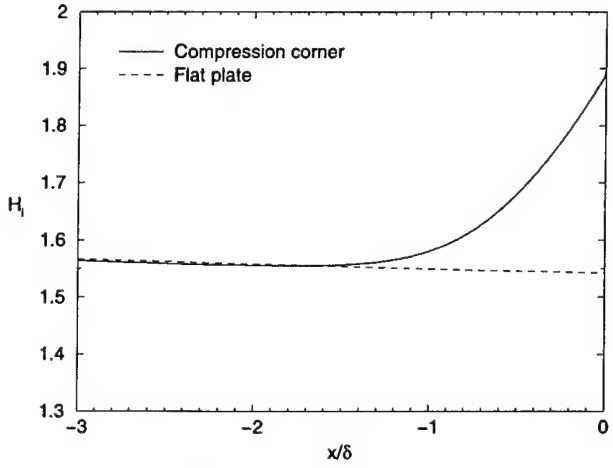

Fig. 25 Shape factor

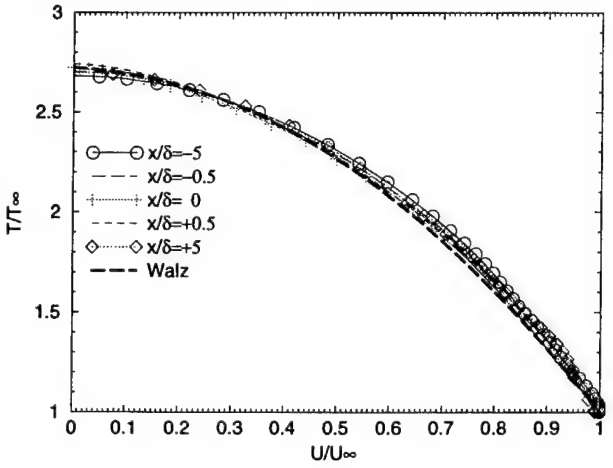

Fig. 26 Mean temperature *vs* velocity

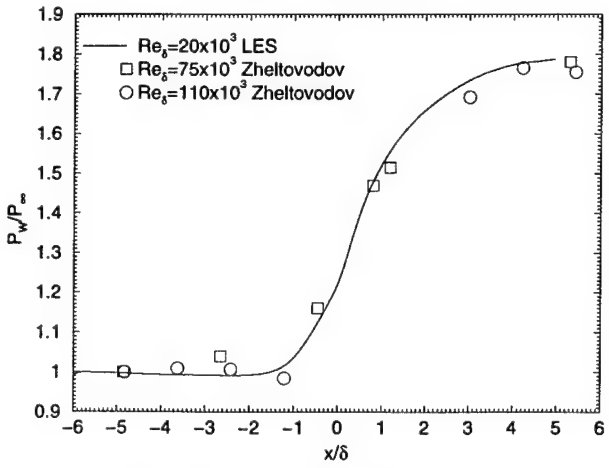

Fig. 27 Mean wall pressure

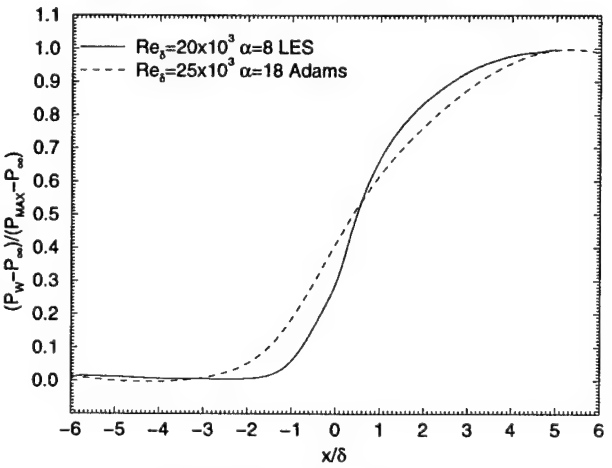

Fig. 28 Mean wall pressure

The incompressible shape factor H_i is displayed in Fig. 25 together with the corresponding result for the supersonic flat plate boundary layer. The initial evolution is identical as expected, indicating that the

upstream boundary is located sufficiently far from the corner to simulate an incoming equilibrium two dimensional turbulent boundary layer flow.

In Fig. 26 the temperature-velocity relationship is evaluated at different stations upstream and downstream of the shock. The simulation data fit well with the classical quadratic profile originally due to Walz (1969).

Fig. 27 displays the mean surface pressure on the wall. The value of Re_δ for the LES and the experiments of Zheltovodov are sufficiently close that the Reynolds number effect should not be significant, and therefore, since the mean flow is unseparated, scaling the distance x by the boundary layer thickness δ is reasonable. Downstream of the shock, the value of the surface pressure reaches the level predicted by the experiments and inviscid theory. Additionally, the slope of the pressure rise seems to be correctly predicted.

A indirect check can be also be performed on the wall pressure. A compression corner at the same Mach number and Reynolds number but higher ramp angle α should provide a smoother pressure gradient, as observed experimentally (Zheltovodov *et al* 1990). The compression corner DNS from Adams (1997) uses the same Mach number, nearly the same Reynolds number, and a different corner angle $\alpha = 18^o$ (Table 4). Fig. 28 compares surface pressure along the wall. The data are here normalized with the downstream pressure level (maximum pressure) in order to take into account the difference in shock strength. The LES using $\alpha = 8^o$ effectively predicts a sharper slope than the DNS using $\alpha = 18^o$.

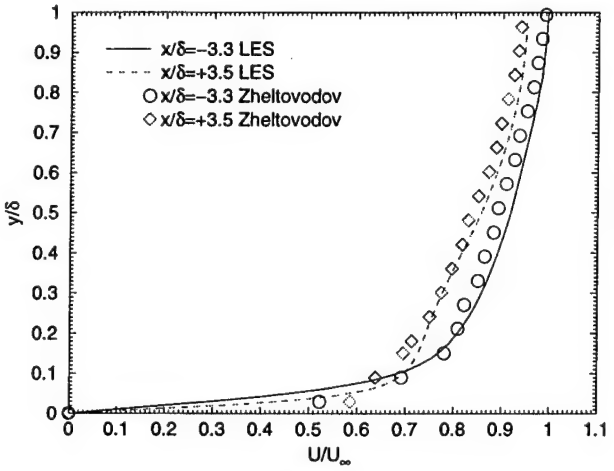

Fig. 29 Mean velocity

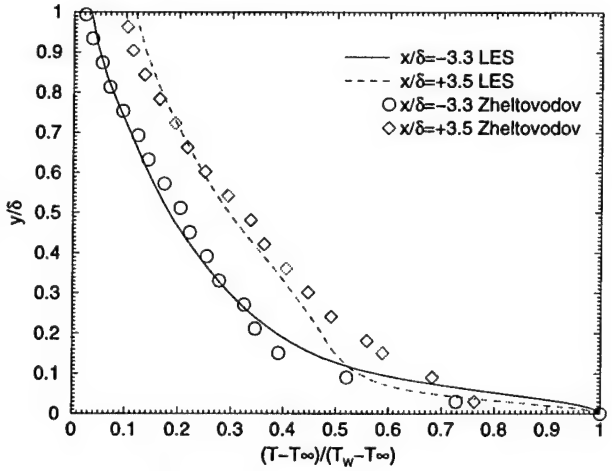

Fig. 30 Mean temperature

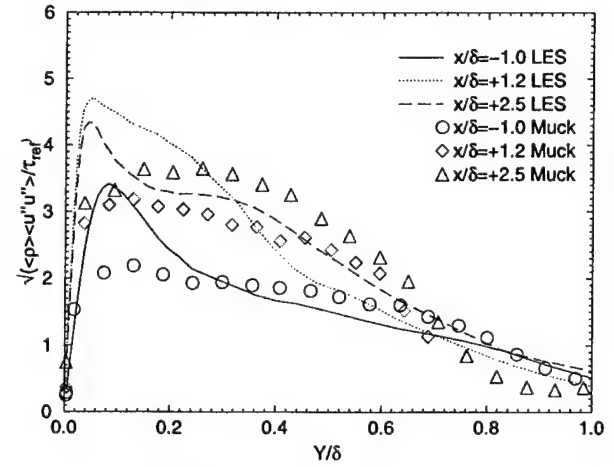

Fig. 31 Reynolds normal stress

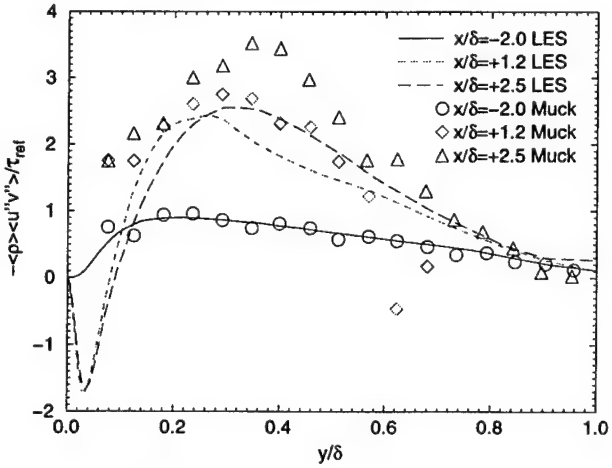

Fig. 32 Reynolds shear stress

The mean velocity at $x/\delta = -3.3$ and 3.5 is shown in Fig. 29. The computed profile displays close agreement with the experimental data of Zheltovodov *et al.* The decrease in velocity due to the shock is well reproduced in the computation except in the immediate vicinity of the wall where the difference between the computed

and experimental Reynolds number is likely to have an effect. The mean static temperature at $x/\delta = -3.3$ and 3.5 is shown in Fig. 30. The agreement between computation and experiment is very good.

The mean streamwise resolved turbulent kinematic normal stress $\ll u''u'' \gg$, normalized using the local mean density $\ll \rho \gg$ and upstream wall shear stress τ_{ref}, is shown in Fig. 31. The reference wall shear stress is constant and measured at $x = -2\delta$. Comparisons are presently shown with Muck *et al* (1984) ($\alpha = 8°$; $M = 3$; $Re_\delta = 1.6 \times 10^6$). In Fig. 32 the Reynolds shear stress distributions are shown for the same experiment. The deformation of these quantities associated with the unfavorable pressure gradient is evident in the vicinity of the corner. Their evolutions show a qualitative agreement. The Reynolds normal stress is amplified by a factor as high as 4. This maximum increase appears at $y/\delta = 0.3$, which is consistent with experiment. The similarity of the experimental data between $0.6 < y/\delta < 1.0$ for different x is also evident in the LES. Similar tendencies and qualitative agreement with the computations are found with the Reynolds normal stress data of Zheltovodov and Yakovlev (1984, 1986), and Zheltovodov *et al* (1990). It is likely linked with the deformation of the large scale structures in the boundary layer. No conclusion can be drawn for the evolution of the typical peak in the near region due to its lack even in upstream experimental data. Essentially the same holds for the Reynolds shear stresses. Their amplifications correspond to experimental predictions.

Fig. 33 Instantaneous density at $z = 2.2\delta$

Fig. 34 Instantaneous temperature at $z = 2.2\delta$

Figs. 33 and 34 show the instantaneous density and temperature contours within the boundary layer in an $x - y$ plane. Large turbulent structures can clearly be seen, both upstream and downstream of the corner where the shock appears.

Bibliography

Adams, N. (1997) "Direct Numerical Simulation of Turbulent Supersonic Boundary Layer Flow", *Advances in DNS/LES - Proceedings of the First AFOSR International Conference on DNS/LES*, Greyden Press, Columbus, OH, pp 29–40, 1997.

Andreopoulos, J. and Muck, K. (1987) "Some New Aspects of the Shock-Wave Boundary Layer Interaction in Compression Ramp Flows", *Journal of Fluid Mechanics*, 180:405–428, 1987.

Ansari, A., and Strang, W. (1996) "Large-Eddy Simulation of Turbulent Mixing Layers", AIAA Paper No. 96-0684.

Bardina, J., Ferziger, J., and Reynolds, W. (1980) "Improved Subgrid Scale Model for Large Eddy Simulation", AIAA Paper No. 80-1357.

Barth, T. (1990) "On Unstructured Grids and Solvers", in *Computational Fluid Dynamics*, Lecture Notes 1990-03, von Karman Institute for Fluid Dynamics.

Barth, T. (1992) "Aspects of Unstructured Grids and Finite-Volume Solvers for the Euler and Navier-Stokes Equations", AGARD Special Course on Unstructured Grid Methods for Advection Dominated Flows, AGARD Report 787.

Boris, J., Grinstein, F., Oran, E., and Kolbe, R. (1992) "New Insights into Large Eddy Simulation" *Fluid Dynamics Research*, Vol. 10, pp. 199–228.

Comte-Bellot, G., and Corrsin, S. (1971) "Simple Eulerian Time Correlation of Full- and Narrow-Band Velocity Signals in Grid-Generated, Isotropic Turbulence", *Journal of Fluid Mechanics*, Vol. 48, Part 2, pp. 273–337.

David, E. (1993) "Modelisation des Ecoulements Compressibles et Hypersoniques : Une Approche Instationnaire", *Ph.D Thesis*, Institut National Polytechnique de Grenoble, France, 1993.

Deardorff, J. (1970) "A Numerical Study of Three Dimensional Turbulent Channel Flow at Large Reynolds Numbers", *Journal of Fluid Mechanics*, Vol. 41, pp. 453–480.

Dolling, D. and Or, C. (1983) "Unsteadiness of the Shock Wave Structure in Attached and Separated Boundary Layers", AIAA Paper 83-1715, 1983.

Eckelmann, H. (1974) "The Structure of the Viscous Sublayer and the Adjacent Wall Region in a Turbulent Channel Flow", *Journal of Fluid Mechanics*, 65:439–459, 1974.

El-Hady, N., Zang, T. and Piomelli, U. (1994) "Applications of the Dynamic Subgrid-Scale Model to Axisymmetric Transitional Boundary Layer at High Speed" *Physics of Fluids* Vol. 6, pp. 1299–1309.

Erlebacher, G., Hussaini, M., Speziale, C., and Zang, T. (1992) "Toward the Large-eddy Simulation of Compressible Turbulent Flows" *Journal of Fluid Mechanics* Vol. 238, pp. 155–185.

Frink, N. (1994) "Recent Progress Toward a Three Dimensional Unstructured Navier-Stokes Flow Solver", AIAA Paper No. 94-0061, 1994.

Galperin, B., and Orszag, S. (1993) "Large Eddy Simulation of Complex Engineering and Geophysical Flows", Cambridge University Press.

Germano, M., Piomelli, U., Moin, P., and Cabot, W. (1991) "A Dynamic Subgrid-scale Eddy Viscosity Model", *Physics of Fluids A*, Vol. 3, pp, 1760–1765.

Ghosal, S., Lund, T., Moin, P., and Akselvoll, K. (1995) "A Dynamical Localization Model for Large Eddy Simulation of Turbulent Flows", *Journal of Fluid Mechanics*, Vol. 286, pp. 229–255.

Gottlieb, J., and Groth, C. (1988) "Assessment of Riemann Solvers for Unsteady One-Dimensional Inviscid Flows of Perfect Gases", *Journal of Computational Physics*, 78:437–458, 1988.

Grinstein, F. (1996) "Dynamics of Coherent Structures and Transition to Turbulence in Free Square Jets", AIAA Paper 96-0781.

Haworth, D., and Jansen, K. (1996) "Large Eddy Simulation on Unstructured Deforming Meshes: Towards Reciprocating IC Engines" Center for Turbulence Research, Stanford University and NASA Ames Research Center.

Hopkins, H. and Inouye, M. (1971) "An Evaluation of Theories for Predicting Skin Friction and Heat Transfer on Flat Plates at Supersonic and Hypersonic Mach Numbers", *AIAA Journal*, 9(6):993–1003, June 1971.

Horstman, C., Settles, G., Vas, I., Bogdonoff, S. and Hung, C. (1977) "Reynolds Number Effects on Shock Wave Turbulent Boundary Layer Interactions", *AIAA Journal*, 15:1152–1158, 1977.

Hunt, D. and Nixon, D. (1995) "A Very Large Eddy Simulation of an Unsteady Shock Wave Turbulent Boundary Layer Interaction", AIAA Paper 95-2212, 1995.

Jansen, K. (1997) "Large Eddy Simulation Using Unstructured Grids", in *First AFOSR International Conference on DNS/LES*, C. Liu and L. Sakell (editors), Louisiana Tech University, Ruston, Louisiana.

Johnson, D. and Rose, W. (1975) "Laser Velocimeter and Hot Wire Anemometer Comparison in a Supersonic Boundary Layer", *AIAA Journal*, 13:512–515, 1975.

Kim, J., Moin, P., and Moser, R. (1987) "Turbulence Statistics in Fully Developed Channel Flow at Low Reynolds Number", *Journal of Fluid Mechanics*, 177:133–166, 1987.

Knight, D. (1993) "Numerical Simulation of 3-D Shock Wave Turbulent Boundary Layer Interactions", AGARD/VKI Special Course on Shock- Wave Boundary-Layer Interactions in Supersonic and Hypersonic Flows, G. Degrez (editor), von Karman Institute for Fluid Dynamics, AGARD R-792, pp. 3-1 to 3-32.

Knight, D. (1994) "A Fully Implicit Navier-Stokes Algorithm Using an Unstructured Grid and Flux Difference Splitting", *Applied Numerical Mathematics*, 16:101–128, 1994.

Knight, D. (1997) "Numerical Simulation of Compressible Turbulent Flows Using the Reynolds-Averaged Navier-Stokes Equations", AGARD Special Course on Turbulence in Compressible Flows", AGARD Report R-819, 1997.

Knight, D., and Degrez, G. (1998) "Shock Wave Boundary Layer Interactions in High Mach Number Flows – A Critical Survey of Current Numerical Prediction Capabilities", AGARD Working Group 18 Report, to appear.

Knight, D., Zhou, G., Okong'o, N. and Shukla, V. (1998) "Compressible Large Eddy Simulation Using Unstructured Grids", AIAA Paper 98-0535, 1998.

Konrad, W. (1993) "A Three Dimensional Supersonic Turbulent Boundary Layer Genereted by an Isentropic Compression", *Ph.D Thesis*, Princeton University, NJ, 1993.

Konrad, W. and Smits, A. (1998) "Turbulence Measurements in a Three-Dimensional Boundary Layer in Supersonic Flow", *Journal of Fluid Mechanics*, 372:1–23, 1998.

Kraichnan, R. (1976) "Eddy Viscosity in Two and Three Dimensions", *Journal of Atmospheric Sciences*, Vol. 33, pp. 1521–1536.

Kreplin, H. and Eckelmann, H. (1979) "Behavior of the Three Fluctuating Velocity Components in the Wall Region of a Turbulent Channel Flow", *Physics of Fluids*, 22(7):1233–1239, 1979.

Lesieur, M., and Métais, O. (1996) "New Trends in Large-Eddy Simulations of Turbulence" in *Annual Review of Fluid Mechanics*, Annual Reviews, Inc., Vol. 28, pp. 45–82.

Lilly, D. (1967) "The Presentation of Small-Scale Turbulent in Numerical Simulation Experiments", *IBM Scientific Computing Symposium on Environmental Sciences*, p. 195.

Lund, T., Wu, X. and Squires, K. (1998) "Generation of Turbulent Inflow Data for Spatially-Developing Boundary Layer Simulations", submitted to *Journal of Computational Physics.*

Mason, P. (1994) "Large Eddy Simulation: A Critical Review of the Technique" *Quarterly Journal of the Royal Meteorological Society* Vol. 120, pp. 1–26.

Menon, S., and Kim, W.-W. (1996) "High Reynolds Numerical Flow Simulation Using the Localized Dynamic Subgrid-Scale Model", AIAA Paper No. 96-0425.

Moin, P., Squires, K., Cabot, W., and Lee, S. (1991) "A Dynamic Subgrid-scale Model for Compressible Turbulence and Scalar Transport", *Physics of Fluids A*, Vol. 11, pp. 2746–2757.

Moin, P. (1997) "Progress in Large Eddy Simulation of Turbulent Flows", AIAA Paper 97-0749.

Muck, K., Spina, E., Smits, A. (1984) "Compilation of Turbulence Data for an 8 degree Compression Corner at Mach 2.9", Report MAE-1642, April 1984.

Muck, K., Dussauge, J., Bogdonoff, S. (1985) "Structure of Wall Pressure Fluctuations in a Shock-Induced Separated Flow", AIAA Paper No. 85-0179, 1985.

Okong'o, N. and Knight, D. (1998) "Compressible Large Eddy Simulation Using Unstructured Grids: Channel and Boundary Layer Flows", AIAA Paper 98-3315, 1998.

Ollivier-Gooch, C. F. (1997) "High Order ENO Schemes for Unstructured Meshes Based on Least Squares Reconstruction, AIAA Paper No. 97-0540, 1997.

Oran, E., and Boris, J. (1993) "Computing Turbulent Shear Flows - A Convenient Conspiracy" *Computers in Physics* Vol. 7, No. 5, pp. 523–533.

Piomelli, U., Cabot, W., Moin, P., and Lee, S. (1991) "Subgrid Scale Backscatter in Turbulent and Transitional Flows", *Physics of Fluids A*, Vol. 3, pp. 1766-1771.

Porter, D., Pouquet, A., and Woodward, P. (1994) "Kolmogorov-like Spectra in Decaying Three-Dimensional Supersonic Flows", *Physics of Fluids* Vol. 6, No. 6, pp. 2133–2142.

Settles, G., Fitzpatrick, T., and Bogdonoff, S. (1979) "Detailed Study of Attached and Separated Compression Corner Flowfields in High Reynolds Number Supersonic Flow", *AIAA Journal*, 17:579–585, 1979.

Smagorinsky, J. (1963) "General Circulation Experiments with the Primitive Equations, I. The Basic Experiment", *Monthly Weather Review*, Vol. 91, pp. 99–164.

Smits, A. and Muck, K. (1987) "Experimental Study of Three Shock Wave / Turbulent Boundary Layer Interactions", *Journal of Fluid Mechanics*, 182:291–314, September 1987.

Smits, A. and Dussauge, J.-P. (1996) *Turbulent Shear Layers in Supersonic Flow*, American Institute of Physics, New York, 1996.

Speziale, C., Erlebacher, G., Zang, A., and Hussaini, M. (1988) "The Subgrid Modeling of Compressible Turbulence" *Physics of Fluids*, Vol. 31, No. 4, pp. 940–943.

Spyropoulos, E., and Blaisdell, G. (1996) "Evaluation of the Dynamic Model for Simulations of Compressible Decaying Isotropic Turbulence", *AIAA Journal* Vol. 34, No. 5, pp. 990–998.

Walz, A. (1969) *Boundary Layers of Flow and Temperature*, MIT Press, Cambridge, 1969.

Yoshizawa, A. (1986) "Statistical Theory for Compressible Turbulent Shear Flows, with the Application to Subgrid Modeling" *Physics of Fluids*, Vol. 29, pp. 2152–2164.

Zang, T., Dahlburg, R. and Dahlburg, P. (1992) "Direct and Large Eddy Simualtions of Three-Dimensional Compressible Navier-Stokes Turbulence" *Physics of Fluids A*, Vol. 4, No. 1, pp. 127–140.

Zheltovodov, A., Schuelein, A., and Yakovlev, V. (1983) "Turbulent Boundary Layer Development Under Conditions of Mixed Interaction with Shocks and Expansion Waves", Preprint No 28-83, Institute of Theoretical and Applied Mechanics, USSR Acad. of Sciences, Novosibirsk, 1983, 51 pg. (in Russian).

Zheltovodov, A., and Yakovlev, V. (1984) "Turbulence Study in Compressible Unseparated and Separated Flows", Report No 1418, Institute of Theoretical and Applied Mechanics, USSR Academy of Sciences, Novosibirsk 1984, 100 pg. (in Russian).

Zheltovodov, A. and Yakovlev, V. (1986) "Stages of Development, Gas Dynamic Structure and Turbulence

Characteristics of Turbulent Compessible Separated Flows in the Vicinity of 2-D Obstacles", Preprint No 27-86, Institute of Theoretical and Applied Mechanics, USSR Academy of Sciences, Novosibirsk, 1986, 55 pg. (in Russian).

Zheltovodov, A., Trofimov, V., Shilein, E., and Yakovlev, V. (1990) "An Experimental Investigation of Supersonic Turbulent Flows in the Vicinity of Sloping Forward and Back Facing Step", Report No 2030, Inst. of Theoretical and Applied Mechanics, USSR Academy of Sciences, Novosibirsk, 1990.

Zheltovodov, A. (1996) "Shock Waves / Turbulent Boundary Layer Interactions - Fundamental Studies and Applications", AIAA Paper 96-1977, 1996.

Personnel and Publications

Personnel

The personnel of the research project are listed in Table 5.

Table 5 Personnel

Name	*Title*	*Period of Participation*	*Supported by*
Prof. Doyle Knight	Principal Investigator	1 Aug 96 - 30 Nov 98	this grant and Rutgers
Ms. Nora Okong'o	Graduate Assistant	1 Aug 96 - 30 Aug 98	this grant and Rutgers
Dr. Gerald Urbin	Postdoctoral Associate	16 Feb 98 - 30 Nov 98	this grant
Dr. Gang Zhou	Postdoctoral Associate	1 Jan 97 - 30 Sep 97	this grant

Papers

Knight, D., Zhou, G., Okong'o, N., and Shukla, V., "Large Eddy Simulation of Compressible Flows Using Unstructured Grids", First AFOSR Conference on DNS/LES, Louisiana Tech University, August 4-8, 1997.

Knight, D., Zhou, G., Okong'o, N., and Shukla, V., "Compressible Large Eddy Simulation Using Unstructured Grids", AIAA Paper No. 98-0535, AIAA 36th Aerospace Sciences Meeting, 1998.

Okong'o, N., and Knight, D., "Compressible Large Eddy Simulation Using Unstructured Grids: Channel and Boundary Layer Flows", AIAA Paper No. 98-3315, AIAA 34th Joint Propulsion Meeting, July 1998.

Urbin, G., Knight, D., and Zheltovodov, A., "Compressible Large Eddy Simulation Using Unstructured Grids: Supersonic Turbulent Boundary Layer and Compression Corner", AIAA Paper No. 99-0427, AIAA 37th Aerospace Sciences Meeting, January 1999.

Papers Submitted

Urbin, G., and Knight, D., "Large Eddy Simulation of the Interaction of a Turbulent Boundary Layer with a Shock Wave using Unstructured Grids", accepted for Second AFOSR International Conference on DNS and LES, June 1999.

Okong'o, N., Knight, D., and Zhou, G., "Large Eddy Simulations Using an Unstructured Grid Compressible Navier-Stokes Algorithm", submitted to *International Journal of Computational Fluid Dynamics.*

Visualization

Zhou, G., Shukla, V., and Knight, D., "Large Eddy Simulation of Decay of Isotropic Turbulence", July 1997.

Okong'o, N., Murray, R., and Knight, D., "Large Eddy Simulation of Turbulent Channel Flow", Nov 1998.

Urbin, G., Murray, R., and Knight, D., "Large Eddy Simulation of Supersonic Compression Corner", Jan 1999.